Supplemental Methods

Supplemental Methods 1: Neural Network Segmentation

A deep learning approach was used to accomplish semantic segmentation of CT images. For training purposes, 9 slices equally spaced in 1 cm increments (the center slice and 8 in the superior-inferior direction) from noncontrast chest CT image volumes in 30 individuals, 15 female and 15 male, reconstructed at 2.5 mm slice resolution (total of 270 slices in the training dataset) were manually segmented using ITK-SNAP.[1]

A conventional neural network approach for medical image segmentation (U-Net)[2] was utilized where the encoder-decoder architecture uses a series of repeated convolutions with downsampling and upsampling to learn salient features in the image which lead to accurate semantic segmentation. We used a U-net with four downsampling and upsampling layers and powers of two for feature depth in each convolutional layer, as depicted in Figure S1. Our U-Net was developed and trained in PyTorch.

The neural network was evaluated using a cross-entropy loss function and was optimized using RMSProp. Five-fold cross validation was performed by splitting the training dataset into 5 subgroups, each with 3 females and males. The networks were optimized using a batch size of 8 slices and were trained for 80 epochs. Mean training and validation loss were logged over the course of training at the end of each epoch and the state of the network was saved to disk. From the five networks and 80 epochs, the network that had the lowest validation loss over the course of training was selected as the model to be used for segmentation in further analysis.

Supplemental Methods 2: Patient-Specific Dose and Imaging Simulation

Let $\mu(\boldsymbol{x}, E)$ be the linear attenuation field where $\boldsymbol{x}$ is the spatial coordinate and E is the photon energy. This linear attenuation field is obtained by semantic segmentation of clinical chest CT images (see Figure S2). Each tissue label was assigned linear attenuation and absorption coefficients derived from the NIST table of X-ray attenuation coefficients[3] and commonly-accepted values for mass density. Also, let $\psi(\gamma)$ be the beam shaping filter attenuation factor where $\gamma(\boldsymbol{x})$ is the angle in the axial plane between $\boldsymbol{x}$ and the central ray on the detector and let $d(\boldsymbol{x}, \beta)$ be the distance from the X-ray source where β is the gantry angle, as shown in Figure S2. Then, the photon flux rate is

$$\phi(\boldsymbol{x}, \beta, E) = \frac{I\phi_o(E)\psi\big(\gamma(\boldsymbol{x})\big)}{d^2(\boldsymbol{x}, \beta)} \exp\left(-\int_{\boldsymbol{x_s}(\beta)}^{x} \mu(\boldsymbol{x}, E)ds\right)$$

where I is the tube current, $\phi_o(E)$ is the source spectrum (in photon counts per mA), and $\boldsymbol{x}_s(\beta)$ is the source position. The exponential term is the 'projection' as shown in Figure S2.

Let $\mu_{\mathrm{en}}(\boldsymbol{x}, E)$ and $\rho(\boldsymbol{x})$ be the linear absorption and mass densities, respectively. The rate of dose absorption (approximated by collison kerma, neglecting scatter) is then given by

$$\dot{u}(\boldsymbol{x}, \beta) = \int \frac{\phi(\boldsymbol{x}, \beta, E)\mu_{\mathrm{en}}(\boldsymbol{x}, E)E}{\rho(\boldsymbol{x})} dE$$

This quantity is depicted as the 'view dose' in Figure S2. Finally, to compute the dose over a complete gantry cycle, we integrate view dose for a full set of views

$$u(\boldsymbol{x}) = \frac{1}{\Omega}\int_0^{2\pi} \dot{u}(\boldsymbol{x}, \beta)d\beta$$

where Ω is the gantry rotation rate. These integrals are accomplished via numerical integration.

Where appropriate, dose is spatially averaged with density weighting. Let $\mathcal{R}$ denote a region in space, then

$$u_{\mathcal{R}} = \frac{1}{\int_{\mathcal{R}} \rho(\boldsymbol{x}) d\boldsymbol{x}} \int_{\mathcal{R}} u(\boldsymbol{x}) \rho(\boldsymbol{x}) d\boldsymbol{x}$$

is the regional dose average.

Since radiation dose u is linearly proportional to X-ray tube current I, dose was quantified by computing the amount of absorbed dose per mA, denoted $U = u/I$.

A similar procedure was performed to simulate the imaging process. This process is depicted in Figure S3. First, the linear attenuation field is forward projected onto a fan-beam detector geometry

$$p(\gamma, \beta, E) = \int_{\boldsymbol{x}_{\mathrm{s}}(\beta)}^{\boldsymbol{x}_{\mathrm{d}}(\gamma,\beta)} \mu(\boldsymbol{x}, \mathrm{E}) \mathrm{d}s$$

where $\boldsymbol{x}_d(\gamma, \beta)$ is the detector position. The expected number of photons detected at each detector position is given by

$$\bar{N}(\gamma, \beta, E) = \frac{I \phi_o(E) \psi(\gamma, E) \eta(E) \Delta}{SDD^2} \exp\big(-p(\gamma, \beta, E)\big)$$

where SDD is the source-detector distance, $\eta(E)$ is the detector efficiency, and Δ is the detector area. The true (stochastic) number of detected photons is determined by a realization of a Poisson random variable $N = \mathrm{Poisson}(\bar{N})$. Similarly, the air scan (no patient in the scanner) is given by

$$N_o(\gamma, E) = \frac{I \phi_o \psi(\gamma, E) \eta(E) \Delta}{SDD^2}$$

The sinogram can then be computed as

$$g(\gamma,\beta) = -\log\left(\frac{\int N(\gamma,\beta,E)E\ dE}{\int N_o(\gamma,E)E\ dE}\right)$$

Images are then reconstructed using fanbeam filtered backprojection with a Ram-Lak filter.

Noise levels are varied by selecting different values for the tube current. We computed the difference between the noisy realization and the noiseless reconstruction to measure the error. Then, we quantified the noise using both the mean squared error (e^2_{MSE}) and the 95th percentile squared error (e^2_{95}) within the region of interest. Owing to the Poisson law, we expect that $e^2 \propto I^{-1}$. This is illustrated in Figure S4. In our analysis, we use linear regression to fit a line to the relationship between tube current and image noise. The slope of the fit m is used to quantify the effect of scanning mode on image quality.

Supplemental References

1. Yushkevich PA, Piven J, Cody Hazlett H, et al. User-Guided 3D Active Contour Segmentation of Anatomical Structures: Significantly Improved Efficiency and Reliability. *Neuroimage*. 2006;31(3):1116-1128.

2. Ronneberger O, Fischer P, Brox T. UNet: Convolutional Networks for Biomedical Image Segmentation. *arXiv Prepr 150504597*. Published online 2015. doi:10.1109/ACCESS.2021.3053408

3. Hubbell JH, Seltzer SM. Tables of X-Ray Mass Attenuation Coefficients and Mass-Energy Absorption Coefficients from 1 keV to 20 MeV for Elements Z=1 to 92 and 48 Additional Substances of Dosimetric Interst. Published online 2004.

Supplemental Figures:

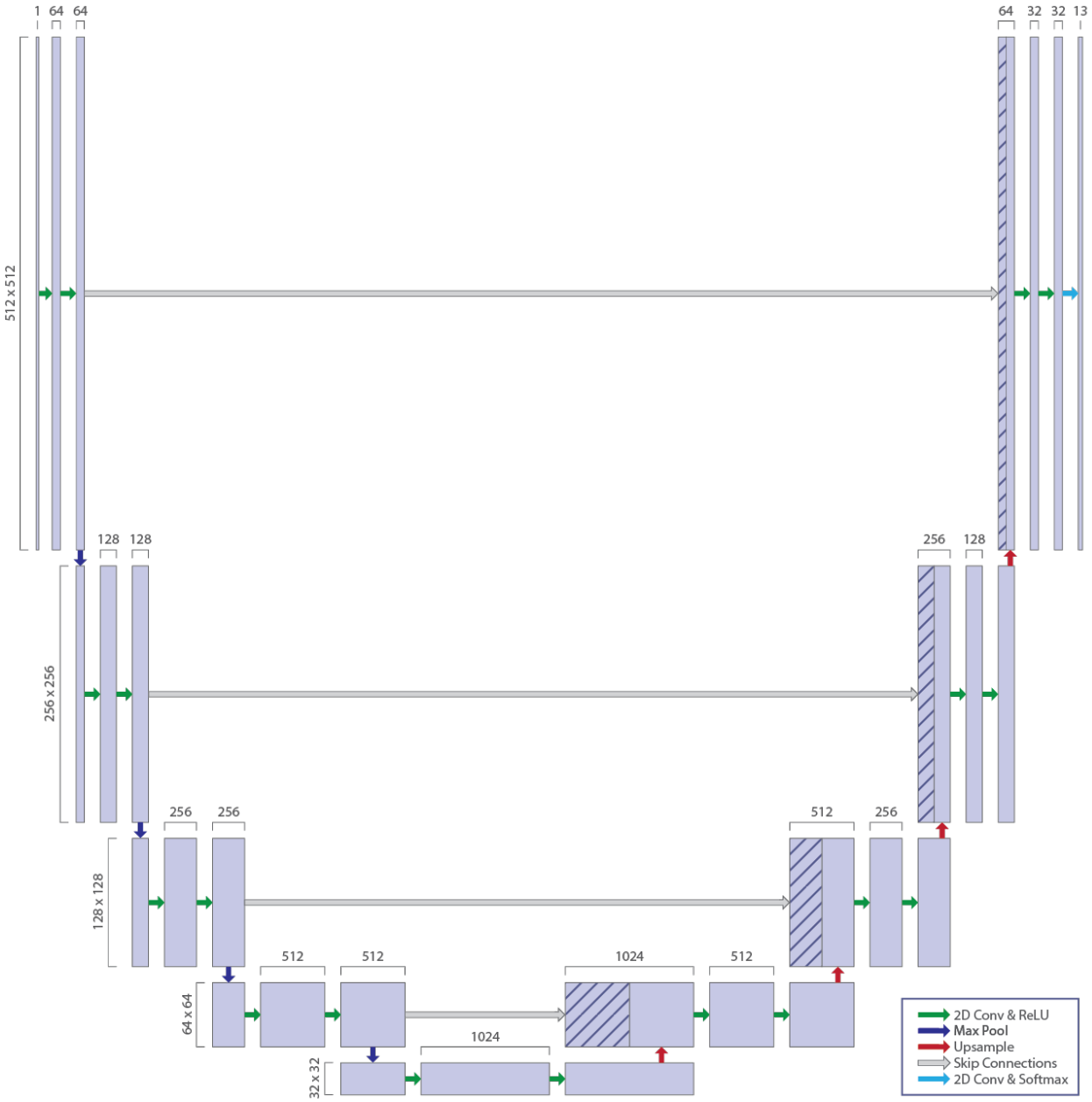

Figure S1: U-Net neural network architecture for semantic segmentation of CT images

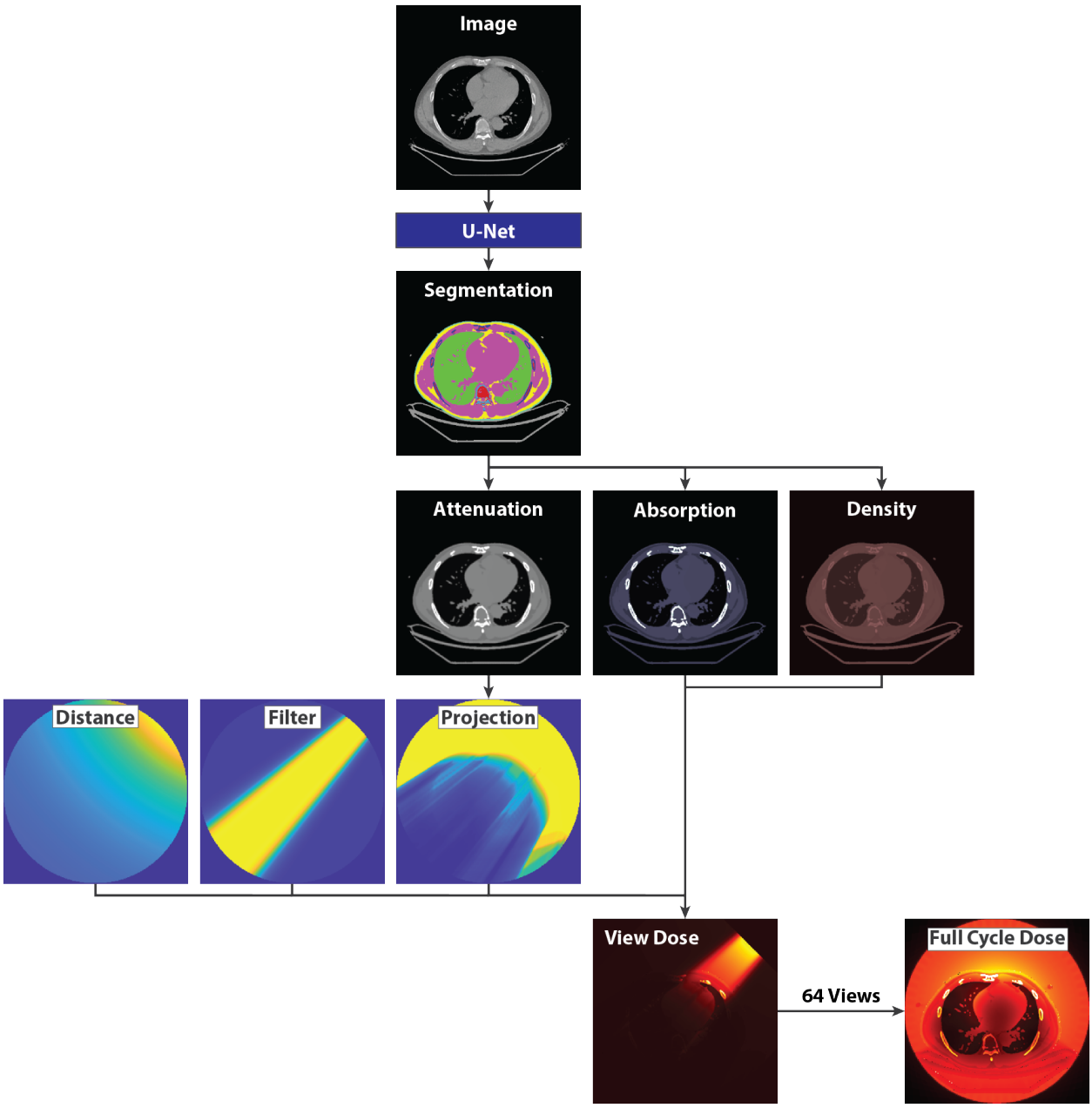

Figure S2: Dose simulation pipeline. The CT images are segmented using a U-Net. Material properties (linear attenuation, linear absorption, and mass density) are assigned according to tissue types. Linear attenuation values are integrated to form the projection which is combined with a filter attenuation profile and inverse-square distance from the source to compute the dose at a given view angle. These view doses are integrated at 64 angles to compute the full cycle dose map.

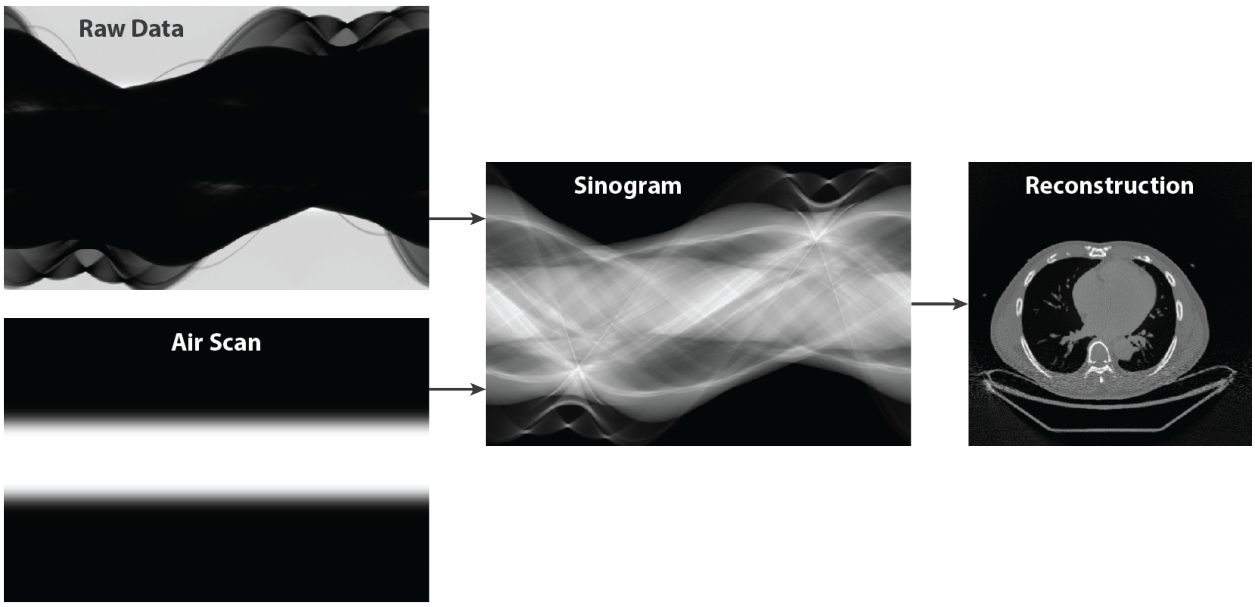

Figure S3: Image simulation pipeline. The central slice of the CT imaging process is simulated. First, a raw count and air scan is computed, then the sinogram is created. The sinogram is finally reconstructed using fanbeam filtered backprojection.

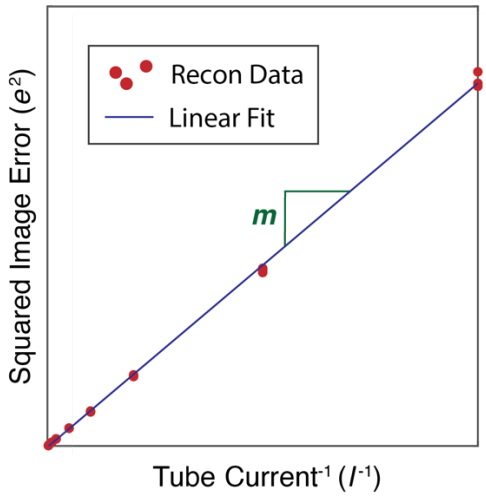

Figure S4: Image noise quantification. Image noise is quantified by the slope of a linear fit of observations of the relationship between tube current and reconstructed image error. The lower this value is, the better the image quality is for a given fluence level.